ResearchGate

See discussions, stats, and author profiles for this publication at: https://www.researchgate.net/publication/237365702

Characterization of ultrathin Ge epilayers on (100) Si

Article *in* Canadian Journal of Physics · February 2011

DOI: 10.1139/p91-041

CITATIONS
4

READS
64

6 authors, including:

D. J. Lockwood
National Research Council Canada
670 PUBLICATIONS **12,472** CITATIONS
SEE PROFILE

Tolek Tyliszczak
Lawrence Berkeley National Laboratory
406 PUBLICATIONS **15,407** CITATIONS
SEE PROFILE

Some of the authors of this publication are also working on these related projects:

Development and applications of Conversion Electron Mossbauer Spectroscopy View project

Composition of wine crystals View project

All content following this page was uploaded by Tolek Tyliszczak on 22 May 2014.

The user has requested enhancement of the downloaded file.

Characterization of ultrathin Ge epilayers on (100) Si[1]

J.-M. BARIBEAU, D. J. LOCKWOOD, AND T. E. JACKMAN
Institute for Microstructural Sciences, National Research Council Canada, Ottawa, Ont., Canada K1A 0R6
AND
P. AEBI, T. TYLISZCZAK, AND A. P. HITCHCOCK
Institute for Materials Research, McMaster University, Hamilton, Ont., Canada L8S 4M1

Received August 14, 1990

The understanding of the epitaxy of pure Ge layers on Si is an important step towards the synthesis of Si_mGe_n (m, $n < 10$ monolayers) short-period superlattices. The possibility of a direct band-gap character makes these structures extremely attractive. We have grown thin buried Ge_n ($1 \leq n \leq 12$ monolayers) films on (100) Si by molecular beam epitaxy and studied their structural properties by a variety of techniques including Raman scattering spectroscopy, glancing incidence X-ray reflection, Rutherford backscattering, transmission electron microscopy, and extended X-ray absorption fine structure analysis. All these techniques allowed detection of the thin Ge layers and provided information about the thickness, morphology, strain distribution, and interface sharpness of these heterostructures. The Ge_n films with $n \leq 5$ had a two-dimensional nature and showed no sign of strain relaxation. Intermixing at the Si–Ge interfaces was present in all these films and estimated to be not more than two monolayers. This smearing at the interfaces may have contributed to the maintenance of that pseudomorphicity. A thicker Ge layer ($n = 12$) showed evidence of strain relaxation and clustering in three-dimensional islands.

La compréhension de l'épitaxie de couches de Ge pur sur Si constitue une étape-importante vers la synthèse de réseaux à courte période Si_mGe_n (m, $n < 10$ monocouches). La possibilité d'un caractère de bande interdite directe rend ces structures extrêmement séduisantes. Nous avons fait croître des films minces enfouis Ge_n ($1 \leq n \leq 12$ monocouches) sur (100) Si par épitaxie de faisceaux moléculaires et étudié leurs propriétés structurales par diverses techniques, dont la spectroscopie de diffusion Raman, la réflexion des rayons X à incidence rasante, la rétrodiffusion Rutherford, la microscopie électronique par transmission et l'analyse de la structure fine d'absorption des rayons X. Toutes ces techniques ont permis la détection des couches minces de Ge et fourni des renseignements sur l'épaisseur, la morphologie, la distribution des contraintes et la netteté des interfaces de ces hétérostructures. Les films Ge_n avec $n \leq 5$ ont une nature bidimensionnelle et ne présentent aucun signe de relaxation des contraintes. Dans tous les films, il y a aux interfaces Si–Ce un mélange qu'on estime ne pas s'étendre à plus de deux monocouches. Ce manque de netteté des interfaces peut avoir contribué au maintien de la pseudomorphicité. Une couche plus épaisse de Ge ($n = 12$) a montré des signes de relaxation des contraintes et d'aggrégation en ilots tridimensionnels.
[Traduit par la rédaction]

Can. J. Phys. **69**, 246 (1991)

Can. J. Phys. Downloaded from www.nrcresearchpress.com by Dalian Nationalities University on 06/05/13
For personal use only.

1. Introduction

In recent years, there has been increasing interest in the synthesis of semiconductor-layered structures of very small vertical dimensions such as short-period superlattices, resonant tunneling diodes, and delta-doped layers. As the thicknesses of the layered structures have been reduced, not only does the synthesis of such microstructures become more difficult, but the structural characterization also becomes a significant challenge. Si_mGe_n (m, $n < 10$ monolayers) short-period superlattices are one example of a thin heteroepitaxial system that has attracted considerable attention because of the possibility of a direct band-gap character that would confer unique optical properties to this Si-based materials system (1). The understanding of the epitaxial growth process of pure Ge layers on Si is an essential step towards the synthesis of these superlattices. We have grown a series of thin buried Ge_n ($1 \leq n \leq 12$ monolayers) films on (100) Si by molecular beam epitaxy (MBE) and studied their structural properties by a variety of techniques including Raman scattering spectroscopy, grazing incidence X-ray reflection, Rutherford backscattering (RBS), cross-sectional transmission electron microscopy (XTEM), and extended X-ray absorption fine structures (EXAFS) analysis. These various techniques were used to study the thin-film morphology, to evaluate the thickness of the buried layers, to estimate the extent of interdiffusion at the Ge–Si interfaces, and to determine the crystalline quality of the heterostructures. The objective of this work is to assess the structural quality of the thin Ge_n layers to identify possible physical limitations that may exist in the growth of Si_mGe_n superlattices.

2. Experiment

The epitaxial layers were grown in a VG Semicon V80 MBE system on 100 mm Czochralski (100) Si wafers. To ensure identical surface conditions, a 150 nm thick Si buffer was first deposited at 515 ± 25°C using optimum growth procedures (2). The substrate was then cooled down to 385 ± 25°C before the thin Ge epitaxial film was grown at a deposition rate of 0.02 nm s^{-1}. The Ge epilayer was immediaely capped with a ~33 nm thick Si layer grown under identical conditions. Six Ge_n layers were prepared with the nominal number of Ge monolayers (ML) n = 1, 2, 3, 4, 6, and 12 (one ML is defined as 0.68×10^{15} atoms cm^{-2}) although the emphasis here is put on the samples with n = 4, 6, and 12.

The absolute amount of Ge was determined using Rutherford backscattering analysis (3) and calibrated Bi-implanted silicon standards (4, 5). The samples were mounted on the multitarget stage of the Ortec 600 scattering chamber and the incident 1.6 MeV $^4He^+$ ions were detected at backscattering angles of 160° and 110°. In addition, the same samples were analyzed using secondary-ion mass spectrometry (SIMS) for the total Ge

[1]NRC No. 32 705.

TABLE 1. Absolute amount of Ge in the various samples

n	RBS/SIMS $n \pm 15\%$	EXAFS* $n \pm 10\%$	Nominal thickness (nm)	Measured thickness (± 0.05 nm)
0	—	—	—	—
4	3.8	3.8	0.58	0.53
6	5.2	5.4	0.87	0.77
12	12.1	12	1.70	1.70

*NOTE: EXAFS data normalized to the 12 ML sample.

content. The measurements were made using the CANMET[2] Cameca IMS-4f ion microscope and previously calibrated Ge-ion implanted standards. A previous study (3) has shown that for sufficiently high incident beam energy (i.e., ion-mixing length), matrix effects are eliminated for these thin buried films. The determined Ge content for each layer, expressed in number of monolayers n, is shown in Table 1. The table also gives the corresponding Ge film thickness calculated assuming that the Ge lattice is tetragonally distorted. Transmission electron microscopy (Philips EM430 operated at 300 kV) was also performed to complement to other techniques used in the investigation.

The glancing incidence X-ray measurements were performed with a Philips 1820 vertical goniometer using Cu K_α radiation. The angular divergence was 0.25° and a receiving slit of 0.1 mm was used. Typically samples of 2–3 cm size were investigated to avoid loss of X-ray intensity and reduce collection of the direct beam near grazing angle.

The Raman spectra of the samples were recorded in a He gas atmosphere in the quasi-backscattering geometry described earlier (6). In this geometry first-order scattering from longitudinal phonons dominates the Raman spectrum. The sample were excited with 300 mW of 457.9 nm argon laser light, while the Raman-scattered light was dispersed with a Spex 14018 double monochromator at a resolution of 3 cm^{-1} and detected with a cooled RCA 31034A photomultiplier. The incident light was polarized in the plane of the incident and scattered light, whereas the scattered-light polarization was not analyzed.

The Ge K-edge (11.1 keV) X-ray absorption spectra of the Ge_n samples were recorded with total electron-yield detection at the C-2 and A-3 beam lines at the Cornell High Energy Synchrotron Source (CHESS). The gas-ionization chamber was operated with He at atmospheric pressure and 100 eV collection voltage (7). The samples were rotated (150–200 rpm) to angularly average and thus eliminate diffraction signals from the Si matrix. The detector was mounted on a two-circle diffraction stage to allow rapid, reproducible variation of the incidence and polarization angles. The spectra reported here were all acquired with small angle of incidence (12° relative to the surface) and with the E-vector of the radiation in the plane of the Ge layer. Spectra recorded with the E-vector perpendicular to the planes were similar but showed some differences, particularly for the thinnest (1 or 2 ML) layers. The polarization dependence of the Ge K-EXAFS of these Ge–Si layers will be reported elsewhere.

3. Results and discussion

3.1. Transmission electron microscopy

Transmission electron microscopy was performed on the various samples to obtain direct structural information. Specimens taken from each wafer were examined in cross section to evaluate the layer thicknesses and compare morphologies. Figure 1 shows cross-sectional views of two Ge_n thin films with $n = 6$ and 12 (nominal values). For the $n = 6$ sample (Fig. 1*a*) as well as for thinner specimens, the buried Ge film appears to be two dimensional and the estimated thickness is in general agreement with the actual values. The contrast at the Si–Ge interfaces is weak suggesting that some interfacial mixing occurs. No dislocations were observed in the Si cap in any of the samples with $n \leq 5$ suggesting that the Ge films are coherently strained.

In contrast the $n = 12$ sample shows clear evidence of three-dimensional growth (Fig. 1*b*). A continuous dark line at the original Si–Ge interface is consistent with an initial layer by layer growth mode. In the uppermost region of the Ge layer, however, dark islands of lateral size of ~10 nm and height 2–5 nm are clearly seen. The dark contrast of these features and defect concentration in their vicinity suggest that they consist of Ge islands. The presence of a high defect density in the Si cap also indicates, as expected, that strain relaxation has occurred in that specimen.

Although XTEM provides direct information on the crystalline perfection of the heterostructures, the absolute amount of Ge in each sample or the extent of interdiffusion at the Si–Ge interface can only be poorly quantified in conventional phase-contrast microscopy.

3.2. Glancing incidence X-ray reflection

For X-ray wavelengths, the refractive index of solids is slightly less than unity and is determined by the surface and near-surface electron density. For glancing incident angles, total external reflection of X-rays occurs making this probe particularly well suited for investigating properties of thin films. Analysis of the reflectivity profile provides an excellent method for extracting structural information such as film thickness, density, and roughness. The thin Ge films were investigated by measurement of intensity oscillations arising from interference between X-rays reflected at the Si–Ge interfaces and at the surface of the Si cap. This technique has a high sensitivity that allows observation of strong interference fringes from buried ultrathin semiconductor films having capping layers only a few tens of nanometres thick.

The reflection amplitude from a multilayer can be calculated using a recurrence relationship to evaluate the reflectivity R_{n+1} at an interface $n + 1$ in terms of the Fresnel coefficients r_{n+1} and the reflectivity R_n from the layer below it. The relevant expression for the reflection amplitude is (8)

$$[1] \quad R_{n+1} = \exp -ik_n d_n \frac{r_{n+1} + R_n}{1 + r_{n+1} R_n}$$

with

$$[2] \quad r_{n+1} = \frac{k_{n+1} - k_n}{k_{n+1} + k_n}$$

$$[3] \quad k_n = \frac{4\pi}{\lambda} (\theta^2 - 2\delta_n - 2i\beta_n)^{1/2}$$

and where θ is the angle of incidence, d_n is the thickness of layer n, and $1 - \delta_n - i\beta_n$ its index of refraction with

$$[4] \quad \delta = \frac{r_e \lambda^2}{2\pi} N(Z + f') \text{ and } \beta = \frac{\lambda \mu}{4\pi}$$

[2]CANMET, Metals Technology Laboratory, Department of Energy Mines and Resources, Ottawa, Ont., Canada K1A 0G1.

Can. J. Phys. Downloaded from www.nrcresearchpress.com by Dalian Nationalities University on 06/05/13
For personal use only.

Can. J. Phys. Downloaded from www.nrcresearchpress.com by Dalian Nationalities University on 06/05/13
For personal use only.

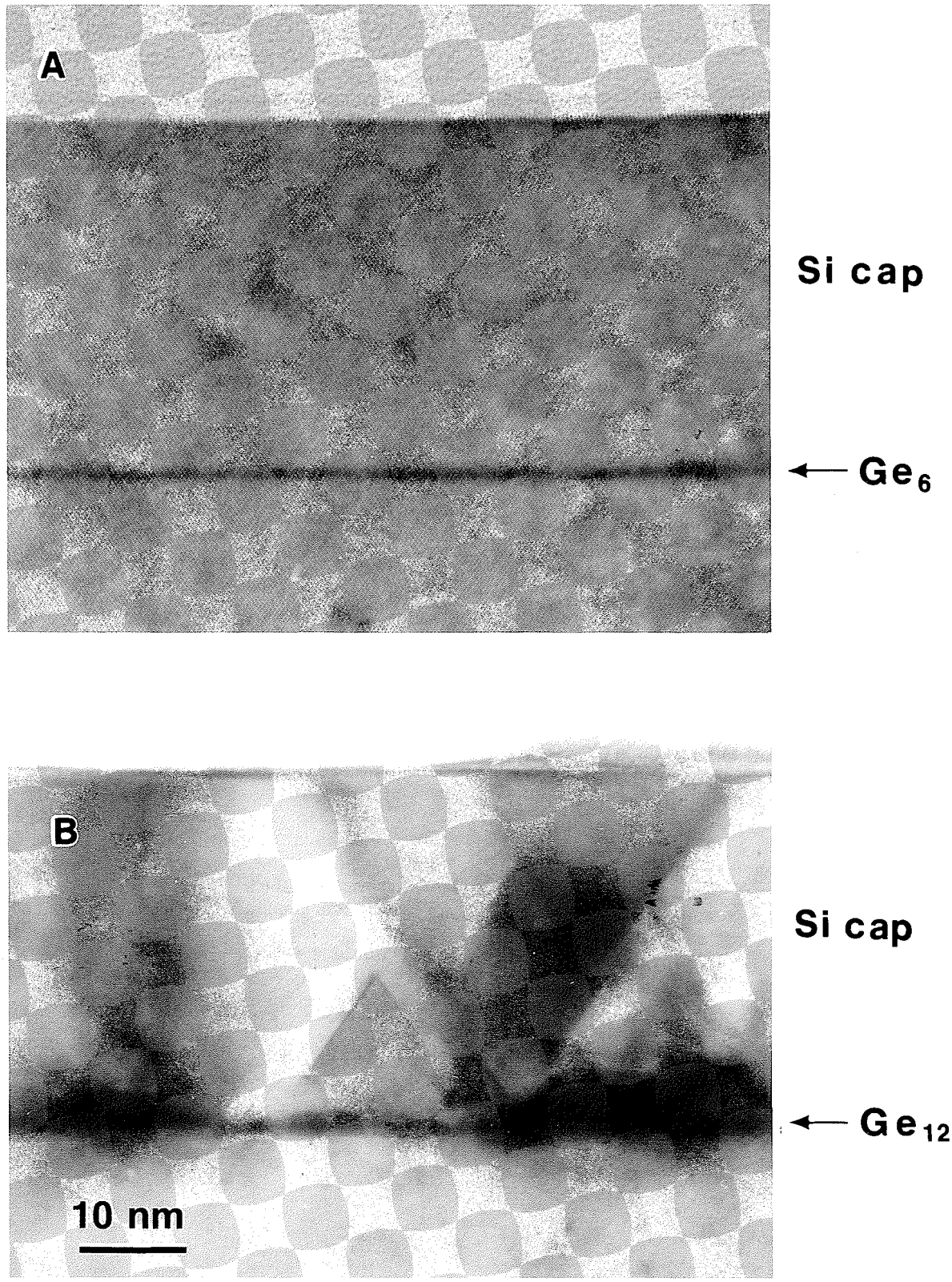

FIG. 1. Transmission electron microscopy cross-sectional views of thin Ge_n films with (A) $n = 6$ and (B) $n = 12$.

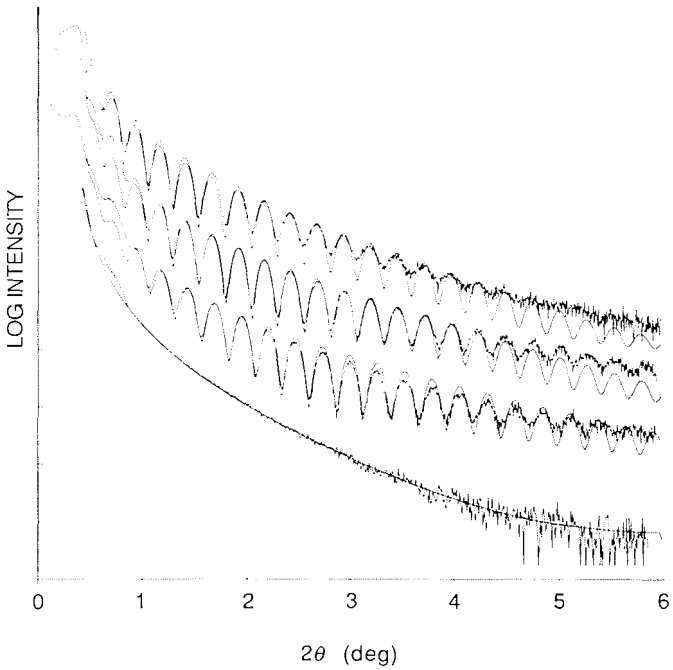

FIG. 2. Normalized experimental and simulated θ–2θ reflectivity curves for thin buried Ge_n layers on (100) Si with from bottom to top (shifted by one decade) $n = 0$, 4, 6, and 12. A constant background of 6×10^{-7} was added to the calculated profiles and a broadening corresponding to an instrumental resolution of about $2\theta = 0.015°$ was introduced.

where N is the atomic density, Z the atomic number, r_e the electron classical radius (2.818×10^{-6} nm), f' the real part of the anomalous absorption, μ the linear absorption coefficient, and λ the X-ray wavelength (0.154 nm). Typically $\delta \sim 1 \times 10^{-6}$ and at grazing incidence, X-rays are totally reflected up to a critical angle $\theta_c = \sqrt{2\delta}$ (9). The roughness at the interface n (σ_n) or at the surface (σ_s) may be taken into account by introducing a Debye–Waller type roughness factor and replacing R_{n+1} in [1] by

$$[5] \quad R'_{n+1} = R_{n+1} \exp -\frac{1}{2} k_n^2 \sigma_n^2 \text{ (or } \sigma_s^2)$$

Finally, an extra contribution from a thin surface oxide layer may be included in the calculation. Notice that the reflectivity does not strongly depend on the strain distribution in the structure (only via a variation of N) and consequently this technique is not suited for studying this physical property.

Figure 2 displays θ–2θ X-ray reflectivity curves measured on a virgin Si substrate and on three thin buried Ge_n layers with $n = 4$, 6, and 12. Figure 2 also presents the corresponding calculated reflectivity curves as obtained from [1]–[3] using values for the Ge thickness (d_{Ge}), Si cap thickness (d_{Si}) and surface roughness (σ_s) listed in Table 2. *No* surface oxide layer was included in the simulation. The uncertainty values in Table 2 indicate the range within which fitting parameters could be varied simultaneously without causing any significant deterioration of the fits.

The reflectivity on the Si substrate exhibits a fast monotonic decrease above the critical angle ($2\theta_c \sim 0.45°$ for Si). Experimental data are very well reproduced when a surface roughness

TABLE 2. Structural parameters used to obtain the calculated profiles of Fig. 2

n	Measured Ge thickness ±0.05 nm	d_{Ge} ±0.10 nm	d_{Si} ±0.05 nm	σ_S ±0.05 nm
0	—	—	subtrate	0.45
4	0.53	0.55	33.0	0.3
6	0.77	0.90	33.5	0.35
12	1.70	1.00	33.5	0.40

$\sigma_s = 0.45$ nm is introduced. Some discrepancy seen below $2\theta = 1°$ is attributed to improper elimination of the direct beam near grazing incidence.

The reflectivity curves from the buried Ge films display sharp periodic oscillations that increase in intensity and shift towards lower angles with increasing Ge thickness. For all the Ge thin films the thickness of the Si cap found in the simulation is about 1 nm larger than values found in the XTEM investigation. This discrepancy is either due to the absence of a surface oxide or contamination layer in the simulation or to a small error in the value of the index of refraction of Si as obtained from [4] owing to impurities or surface effects. In all cases the surface roughness is comparable with that obtained on the Si substrate indicating that the epitaxial growth does not introduce a significant roughening on the scale of the X-ray coherence length (1–10 μm).

The Ge film thicknesses found in the simulations agree with the measured values within one monolayer for all the samples except the 12 ML sample where some damping of the higher angle oscillations is also apparent. For the latter, best agreement is obtained using a Ge thickness of about half the actual value. This thickness provides a very good fit of the intense oscillations at low angles but produces too much intensity modulation at high angles. This result is consistent with the XTEM investigation that showed that this Ge layer exhibits a transition from two-dimensional to three-dimensional growth at a coverage of ~6 ML. In such circumstances only the X-rays reflected at the surface of a two-dimensional film of about 6 ML thickness should contribute to the interference process. The uppermost Ge islands being randomly distributed and varying in size and height should not give rise to any well-defined intensity oscillations but rather may cause a smearing of the fringes originating from the underlying Ge layers. Presence of misfit dislocations at the Ge–Si interface, as evidenced by XTEM, produces local lattice misorientations that may also have contributed to reducing the amplitude of the X-ray interference fringes. Attempts to include a surface oxide or contamination layer in the simulation or introduction of smearing at the Ge–Si cap interface using [5] did not provide any significant improvement of the fits. The use of such a smearing factor is, in any case, questionable for such thin buried layers. In fact, X-ray reflectivity is not sensitive to interface smearing on the atomic step scale. For example, the reflectivity from a $Si_{0.5}Ge_{0.5}$ buried film twice the thickness of a pure Ge layer would exhibit very analogous intensity oscillations because both layers introduce a similar wave-function phase shift. Lattice strain and interdiffusion are more easily studied by techniques sensitive to the local atomic arrangement such as Raman spectroscopy or EXAFS. The glancing incidence X-ray measurements will be discussed in more detail elsewhere (J.-M. Baribeau, manuscript in preparation).

Can. J. Phys. Downloaded from www.nrcresearchpress.com by Dalian Nationalities University on 06/05/13
For personal use only.

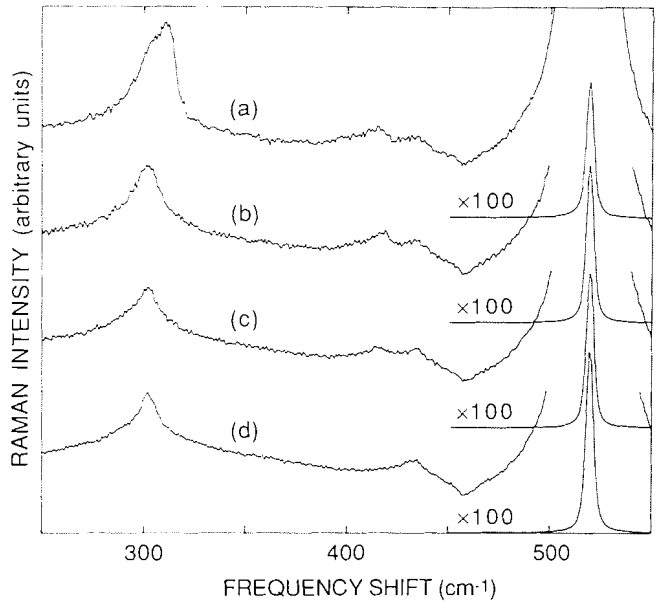

FIG. 3. Raman spectra of the optic phonons of (*a*) $n = 12$, (*b*) $n = 6$, and (*c*) $n = 4$ Ge_n samples, and (*d*) the Si substrate ($n = 0$). The intense peak at 520 cm^{-1} is due to the Si buffer and capping layers.

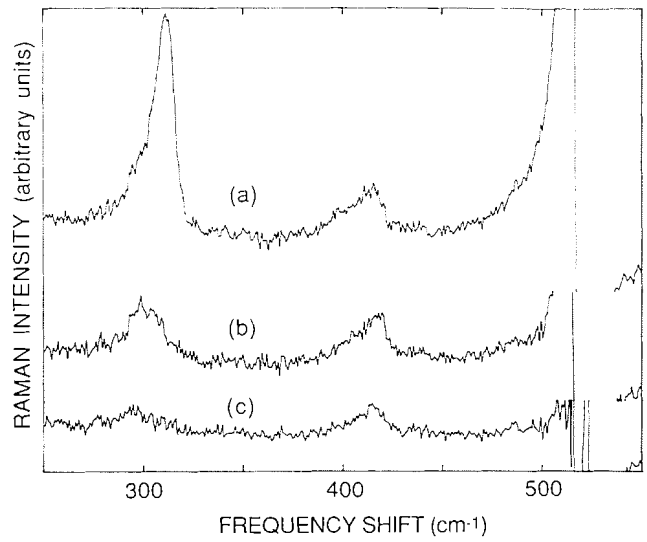

FIG. 4. Raman spectra of the Ge_n layers for (*a*) $n = 12$, (*b*) $n = 6$, and (*c*) $n = 4$ samples revealed by the subtraction process described in the text.

3.3. Raman scattering spectroscopy

Earlier experimental and theoretical work on thick and ultrathin layer superlattices of Si–Ge (6, 10) has shown that current lattice dynamical models for the acoustic- and optic-phonon frequencies in these structures are in good accord with experiment. For thick layer superlattices, the layer thicknesses and intralayer strain may be deduced from the Raman spectrum with the aid of these models (6). The same information may also be obtained from theoretical analyses of the atomic-layer superlattice spectra, but here the interpretation is made more complicated by the now significant effects of interface blurring on phonon frequencies and intensities (11). The analysis of the Raman spectrum is dependent to some extent on the model used to represent the physical form of the interface in a particular sample. Nevertheless, the experience gained in the earlier studies, particularly of phonons in structures with abrupt interfaces where strain and confinement effects may be clearly delineated (10), provides a useful starting point for analyzing the Raman spectra of the Ge_n samples.

The optical-phonon Raman spectra of three Ge_n samples with $n = 4$, 6, and 12 are shown in Fig. 3. The dominant peak at 520 cm^{-1} is largely due to the Si buffer layer, as the 457.9 nm exciting light is strongly absorbed in Si (6) and does not reach the Si substrate. A small contribution to the signal near 520 cm^{-1} also comes from the relatively thin Si capping layer. The optical phonon from the capping layer may be at a slightly different frequency from the buffer and substrate line if the capping layer is strained. However, it is difficult to extract any information about the capping layer from its contribution to the Raman spectrum, because it is dominated by the underlying bulk-Si signal. The weaker peak near 300 cm^{-1} is a mixture of contributions from the pure Si second-order spectrum (see Fig. 3) and Ge–Ge vibrations within the Ge_n layer (11, 12). Finally, the even weaker peaks near 400 and 425 cm^{-1} are, respectively, due to Ge–Si vibrations associated with Si next to (or within) the Ge_n layers (13) and a second-order Si feature (see Fig. 3).

The spectral features arising from the Ge_n layer simply add on to other features due to the Si cap and buffer layers and may be revealed by subtracting the Si spectrum. In the present case the spectrum from the Si substrate material shown in Fig. 3 was scaled to the 520 cm^{-1} peak in the Ge_n-layer spectra of Fig. 3 and subtracted. The results of the subtractions are given in Fig. 4. The subtraction of the strong 520 cm^{-1} line is not perfect, as evidenced by the large oscillation near 520 cm^{-1}, which could be due to the fact that the Si cap and buffer-layer spectrum is possibly not identical to the Si substrate spectrum. Nevertheless, the subtractions have eliminated the weaker second-order Si features and have revealed the intrinsic optical phonons in the Ge_n layers with sufficient accuracy. The peak frequencies of these phonons are listed in Table 3.

It has been shown from theoretical studies of Si–Ge atomic layer superlattices (14) that a Ge–Si Raman peak near 400 cm^{-1} should *not* be observable in the backscattering geometry for systems with perfect interfaces. Such peaks are, in fact, commonly seen in the Raman spectra of such superlattices, because the materials do not have perfectly abrupt Si–Ge interfaces (15). Thus the Ge–Si line observed near 415 cm^{-1} in our samples indicates imperfect Si–Ge interfaces. The line is relatively weak and of similar frequency and intensity in each sample suggesting that the degree of interface disorder is small and that it occurs to a similar extent in each sample. The peak is asymmetric in shape having a shoulder on the low-frequency side in each case (see Fig. 4). The double-humped disposition of the interface peak is characteristic of interface roughness (16).

The Ge–Ge peak on the other hand shows considerable variations in the frequency and intensity with n. For $n = 12$, the peak frequency lies above the bulk Ge value of 301 cm^{-1}, but decreases below 301 cm^{-1} for $n = 6$ and 4. The confinement effect of sandwiching the Ge epilayer within the Si layers lowers the Ge–Ge phonon frequency from the bulk value, while both strain and interface roughness act to increase the Ge–Ge phonon frequency (11, 15). In the thicker $n = 12$ layer, where the Ge–Ge line frequency exceeds the bulk value by ~4%, the effect of confinement is less significant and it is clear that lattice strain and(or) interface roughness are dominating and are

Can. J. Phys. Downloaded from www.nrcresearchpress.com by Dalian Nationalities University on 06/05/13
For personal use only.

TABLE 3. Peak frequencies of longitudinal optical phonons in the Raman spectra of Ge_n layers buried in Si

	Frequencies (cm^{-1})	
n	Ge–Ge	Ge–Si
4	294.4	414.7
6	298.3	417.0
12	311.4	414.5
Bulk Ge	301	—

responsible for the overall upward shift in frequency. The XTEM analysis has shown that the $n = 12$ layer is not homogeneous and that the Si cap is heavily dislocated. The Raman sampling area ($\sim 0.1 \times 1$ mm^2) is large enough that the observed spectrum contains features due to all of the different configurations within the Ge layer (i.e., ranging from epitaxial strained layers near the Si-buffer–Ge-layer interface to relaxed three-dimensional islands). It is thus not surprising that the line at 311 cm^{-1} in Fig. 4 has an asymmetric line shape. This line appears to comprise largely two components one of which could be due to the islands (the shoulder near 300 cm^{-1}) and the other (the main peak) due to partially relaxed epitaxial layers. Such an interpretation is consistent with the growth model of Eaglesham and Cerullo (17) and with the X-ray diffraction analysis of strain relaxation of Macdonald *et al.* (18). If this interpretation of the 311 cm^{-1} line is correct, then the 311 cm^{-1} line is the composite Raman signal of epitaxial Ge layers strained to varying degrees, but always less than that expected from the Si–Ge lattice mismatch. In this case it is probable that interface roughness is the major factor in producing the upward shift of the Ge–Ge line.

The $n = 4$ and 6 cases are more problematic, because all three factors (strain, confinement, and interface roughness) must be considered. Recent calculations for a perfect Si–Ge_n–Si-cap (5 nm thick) sandwich (11) indicate a Ge–Ge peak frequency of 284 and 295 cm^{-1} for the $n = 4$ and $n = 8$ cases, respectively, with a strain imposed by a 10% increase in the Ge layer force constants raising the respective frequencies to 297 and 307 cm^{-1}. The experimental results given in Table 3 are within this range.

Assuming that the Raman intensity of the Ge–Ge line is proportional to the Ge layer thickness, the $n = 12$ line is approximately twice as strong as would be expected from the $n = 4$ and 6 results. This implies that not all of the Ge_n layers are pure Ge. If we assume that the observed intensity variation is due to interface blurring only, then the Raman results show that the interface roughness on the Ge side of each Si–Ge interface due to Si inclusions is not more than two monolayers in size.

3.4. EXAFS

One of the motivations for the X-ray absorption measurements was to use the local structure sensitivity of the EXAFS signal to determine the dependence, on layer thickness of the relative numbers, of Ge and Si in the first co-ordination shell about Ge. This would then provide an independent check on the results based on the local mode intensities observed by Raman scattering as discussed in the preceding section.

X-ray absorption spectroscopy (XAS) has been revitalized with the advent of intense synchrotron radiation sources, which allow studies of rather dilute samples. In addition to quantitative element analysis, the extended fine structure (EXAFS)

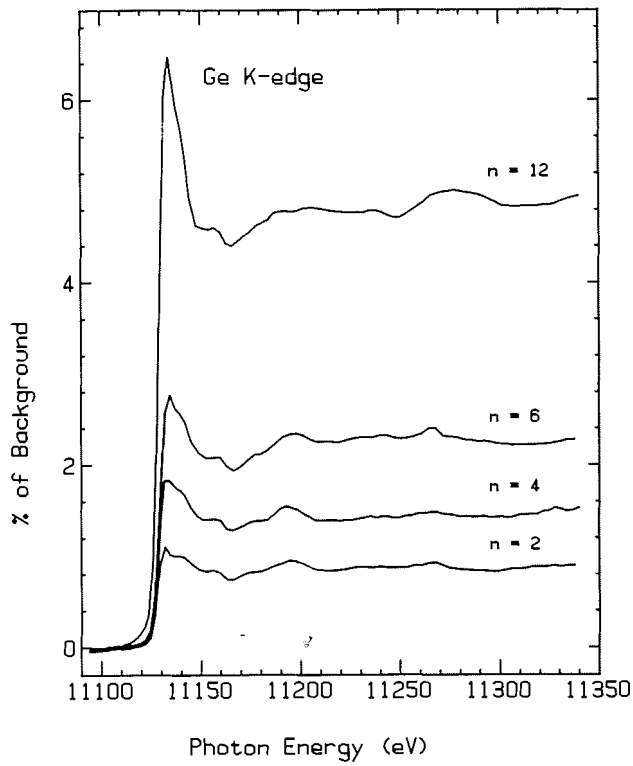

FIG. 5. Background subtracted Ge K-edge X-ray absorption spectra of Ge_n samples ($n = 2, 4, 6$, and 12) plotted on a common scale. The spectra were recorded at the C-2 and A-3 beam lines at CHESS using total electron yield detection and sample rotation to remove diffraction artifacts. The vertical scale indicates percentage of background at the edge.

component of the XAS signal can provide a quantitative local structure information (19). In a single scattering description the EXAFS signal, which is the energy-dependent interference between the outgoing and backscattered photoelectron wave, is (20):

$$[6] \quad \chi(k) = \sum_i \chi_i(k) = \sum_i A_i \frac{N_i}{k^2 r_i^2} \exp(-2k^2\sigma_i^2) \sin[2kr_i + \varphi_i(k)]$$

where $A_i(k)$ is the backscattering amplitude as a function of wave number k (Å^{-1}) $= \sqrt{0.263(E - E_0)}$ (1 Å $= 10^{-10}$ m) where E_0 is the photon energy (in eV) at which the photoelectron has zero kinetic energy) from each of the neighboring atoms of type i, which are located at a distance r_i and have a mean-square relative displacement σ_i^2. This expression assumes Gaussian distributions of interatomic distances and ignores inelastic intensity losses and multiple scattering. Calculated spherical wave-amplitude and phase functions (21), which are frequently used to estimate the $A_i(k)$ and $k_i(k)$ functions, are needed to derive quantitative distances and co-ordination numbers from experimental EXAFS data. k-space fitting procedures (19, 20) are necessary for analyses of materials in which the first co-ordination shell is a mixture of several elements, as in the case of the Ge_n samples. With good-quality EXAFS data, distances accurate to 0.02, co-ordination numbers to 20% and elemental identity to $\pm 2Z$ units (through the shape of the back-

Can. J. Phys. Downloaded from www.nrcresearchpress.com by Dalian Nationalities University on 06/05/13
For personal use only.

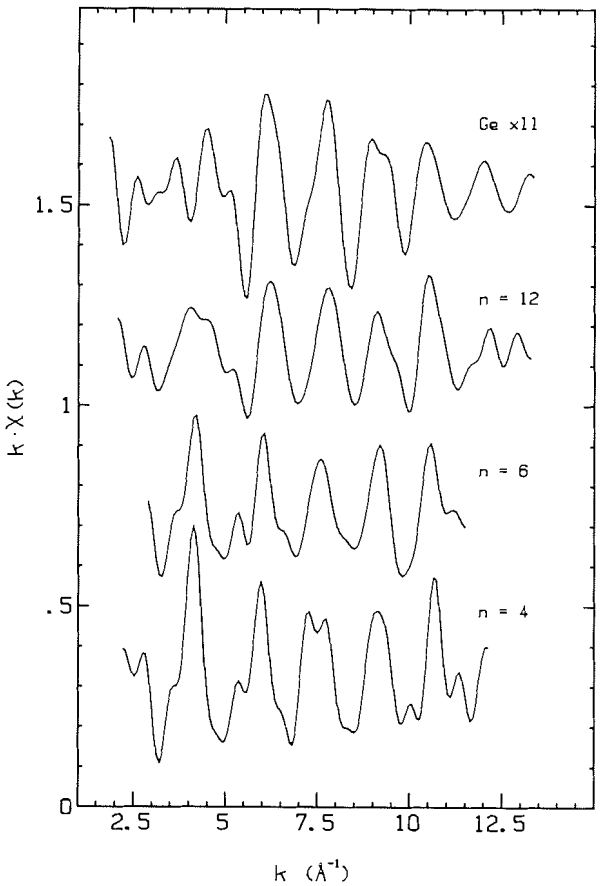

FIG. 6. k^1-weighted extended fine structure spectra extracted from the K-edge X-ray absorption spectra of Ge_n samples (n = 4, 6, and 12) and pure Ge.

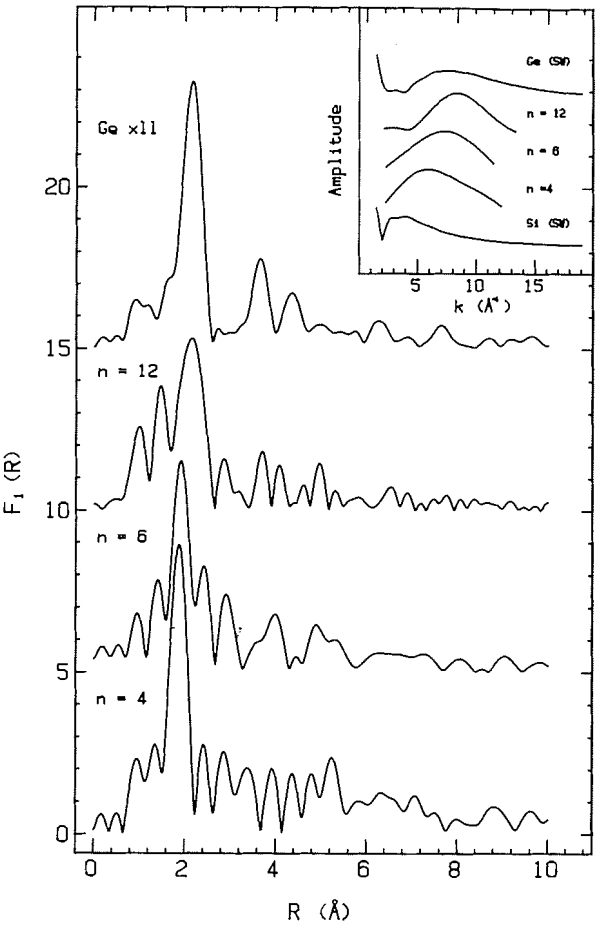

FIG. 7. Magnitude of the Fourier transforms of the Ge K-EXAFS of Ge_n samples (n = 4, 6, and 12). The insert compares the Fourier filtered first-shell backscattering amplitudes (1.2–1.4 Å) for the n = 4, 6, 12 samples with the calculated backscattering amplitude of pure Ge and Si (21).

scattering amplitude function) can be obtained for the first co-ordination shell (21). Since the Ge_n layers in the present samples constitute a very dilute sample for EXAFS, the quality of the data unfortunately limits the precision of the results. Recently the technique has been applied to studies of As doped Si (22–24). Although the local concentration of Ge in the Ge–Si monolayers is much larger than for the Si(As), the total number of atoms contributing to the signal is of a similar order of magnitude.

Figure 5 presents the Ge K-edge spectra following background subtraction for the same n = 4, 6, and 12 samples used in the Raman scattering measurements, along with that for a Ge single crystal. The relative amount of Ge in the Ge_n layers was determined from the height of the absorption-edge jump. This is compared in Table 1 with values derived from the SIMS and Rutherford backscattering measurements. All values agree within the precisions of the individual measurements. One notes from Fig. 5 that the shape of the near-edge features are rather similar in all spectra (consistent with similar tetrahedral first shell co-ordination around Ge). However, the intensity of the white line (11 135 eV) relative to the continuum in the n = 12 sample is 1.40, which falls between the values for pure Ge (1.52) and the other samples (1.31). This is consistent with the conclusion that for the n = 12 sample three-dimensional islands of Ge have formed. Although the details differ, the near edge region is found to be a valuable adjunct to EXAFS as was the case for Si(As) (24).

The $k^1\chi(k)$ Ge K-EXAFS of the n = 2, 4, 6, and 12 samples are presented in Fig. 6 along with that of pure Ge. Each of these spectra are the sum of 2 or 3 separate spectra each obtained in ~10 min. A broad Fourier filter (1–6 $Å^{-1}$) has been used to remove high-frequency noise in the $k^1\chi(k)$ presentation. Figure 7 presents the magnitudes of the Fourier transforms (FTs) of the data shown in Fig. 6. For each single-layer sample the FTs are dominated by the first-shell signal. Analysis of the amplitude shapes indicates that this signal has contributions from both Si and Ge backscatters in all cases. While we have not yet completed the k-space curve fit analysis of this data to determine quantitatively the proportion of Si and Ge in this first shell for each sample (nor have we determined the confidence level with which the program can extract this information in such a dilute system), qualitatively there is clear evidence for a shift from a Si-dominated to a Ge-dominated first coordination shell as the thickness of the layer increases. This is presented in the insert to Fig. 7, which presents the Fourier-filtered first-shell amplitudes (1.2–1.4 Å in k-space) in comparison with calculated spherical-wave backscattering amplitudes for pure Si and Ge (21).

Relative to the Ge K-EXAFS of single crystal Ge (Fig. 7), the signal in the FT at distances beyond the first shell is much less well defined. This is true even for the n = 12 sample where

Can. J. Phys. Downloaded from www.nrcresearchpress.com by Dalian Nationalities University on 06/05/13
For personal use only.

Can. J. Phys. Downloaded from www.nrcresearchpress.com by Dalian Nationalities University on 06/05/13
For personal use only.

one might expect a large fraction of the Ge atoms to be in an environment very similar to that of single crystal Ge. In fact, the EXAFS of the thinner layers shows a larger second shell distance (i.e., signal between 2.5 and 4.0 Å) than the thicker layers. This suggests that for these thicknesses, the growth procedures achieved epitaxy with good lattice matching between the Ge layer and the Si (100) subtrate. On the other hand the structure at the level of the next nearest neighbors appears strongly distorted in the thick layer. This is consistent with a rapid increase in the defects as the layer relaxes.

We note that the present results are significantly different from grazing incidence fluorescence measurements of Ge_nSi (n = 2, 4, and 8) monolayer superlattices recently reported by Oyangi *et al.* (24). The Ge *K*-EXAFS in that work is very similar to that for bulk Ge, with strong higher shell signal, particularly in the n = 8 sample. The large difference between their results and ours can only be explained by significant interdiffusion at our Si–Ge interfaces.

4. Conclusions

Owing to modern growth technologies such as MBE, growth of atomic layer thick heterostructures can now be attempted. In this work we have discussed the growth and characterization of ultrathin buried Ge_n layers on (100) Si. To fully assess such thin microstructures it is essential to resort to complementary analytical techniques sensitive to different physical properties of the thin film. Glancing incidence X-ray reflection, RBS, Raman scattering spectroscopy, EXAFS, and transmission electron microscopy have all the sensitivity required for detecting monolayer thick buried Ge layers. However, only a correlation of the results obtained with these various techniques allows a thorough materials characterization. For example, RBS or X-ray reflection allow an accurate measurement of the Ge coverage but lack monolayer-depth resolution and strain sensitivity. Information on these properties can be obtained by Raman scattering and EXAFS, which are both sensitive to the chemical environment via the interatomic bond lengths. Finally, transmission electron microscopy is best suited to study the thin-film structural perfection and morphology. The main results of the present investigation can be summarized as follows:

(*i*) Although little diffusion is expected in an heterostructure grown at a temperature below 400°C, buried Ge_n thin layers show evidence of interdiffusion at the Si–Ge interfaces over one or two monolayers. This result suggests that surface dynamics plays a crucial role in determining the degree of abruptness of solid-state interfaces.

(*ii*) Two-dimensional Ge films, with no evidence of relaxation, were found up to a coverage of at least five monolayers. This value exceeds the equilibrium critical thicknesses for pseudomorphic growth (18, 26–28), which is estimated to be 3–4 ML for the Ge–Si system. Interfacial mixing may have contributed to reducing the strain and surface energy and allowing two-dimensional growth to thicknesses exceeding the equilibrium critical values. Coherent two-dimensional growth of Ge on (100) Si up to a thickness of ~6 ML has also been reported by several authors (17, 29)

(*iii*) Ge clustering and strain relaxation were observed in a 12 monolayer Ge buried layer. This three-dimensional growth process may be connected with the onset of strain relaxation of the heterostructure.

(*iv*) The Raman results are consistent with the proposed model (17) of a variation in strain in Ge layers thicker than the critical value.

From the above conclusions it is clear that the epitaxy of Si_mGe_n superlattices may be hindered by serious fundamental limitations. Although three-dimensional growth may be avoided by limiting the thickness of individual layers to 5–6 ML, substantial interdiffusion, possibly affecting the zone-folding properties of the heterostructures, may still be present. Other phenomena such as strain enhancement of interdiffusion (30, 31) or long-range ordering (32–34) may add to the difficulty of synthesizing and processing these artificial structures. These difficulties may be overcome by restricting the growth kinetics even further (i.e., lower growth temperature or higher deposition rate). This may however result in a loss of crystallinity that could require post-growth processing. Use of surfactants (35) to modify the surface energy has been found efficient for achieving two-dimensional growth of Ge on Si and certainly deserves more investigation.

Acknowledgements

We thank J. P. McCaffrey for the transmission electron microscopy analysis and H. J. Labbé for the Raman scattering measurements. Financial support was provided by the Natural Sciences and Engineering Research Council of Canada and the Ontario Centre for Materials Research. We thank the dedicated staff scientists and operators at the CHESS, especially Dr. K. Finkelstein, for their assistance.

1. E. Kasper and E. H. C. Parker (*Editors*). Silicon molecular beam epitaxy. North-Holland Publishing Co., Amsterdam. 1989.
2. J.-M. Baribeau, T. E. Jackman, P. Maigné, D. C. Houghton, and M. W. Denhoff. J. Vac. Sci. Technol. A, **5**, 1898 (1987).
3. J. A. Jackman, L. Dignard-Bailey, R. S. Storey, C. Macpherson, S. Rolfe, L. Van der Zwan, and T. E. Jackman. Nucl. Instrum. Methods, B, **45**, 592 (1990).
4. C. Cohen, J. A. Davies, A. V. Drigo, and T. E. Jackman. Nucl. Instrum. Methods, **218**, 147 (1983).
5. T. E. Jackman, J. A. Davies, and D. Chivers. Nucl. Instrum. Methods B, **19/20**, 345 (1987).
6. D. J. Lockwood, M. W. C. Dharma-wardana, J.-M. Baribeau, and D. C. Houghton. Phys. Rev. B: Condens. Matter, **35**, 2243 (1987).
7. T. Tyliszczak and A. P. Hitchcock. Physica B, **158**, 335 (1989).
8. L. G. Parratt. Phys. Rev. **95**, 359 (1954).
9. A. Segmüller. Thin Solid Films, **18**, 287 (1973).
10. G. Fasol, A. Fasolino, and P. Lugli (*Editors*). Spectroscopy of semiconductor microstructures. Plenum Publishing Corp., New York. 1989.
11. M. W. C. Dharma-wardana, G. C. Aers, D. J. Lockwood, and J.-M. Baribeau. *In* Light scattering in semiconductor structures and superlattices. *Edited by* D. J. Lockwood and J. F. Young. Plenum Publishing Corp., New York. 1991.
12. J. C. Tsang. *In* Spectroscopy of semiconductor microstructures. *Edited by* G. Fasol, A. Fasolino, and P. Lugli. Plenum Publishing Corp., New York. 1989. p. 175.
13. J. Menéndez, A. Pinczuk, J. Bevk, and J. P. Mannaerts. J. Vac. Sci. Technol. B, **6**, 1306 (1988); S. Wilke. Solid State Commun. **73**, 399 (1990).
14. E. Molinari and A. Fasolino. Appl. Phys. Lett. **54**, 1220 (1989).
15. M. W. C. Dharma-wardana, G. C. Aers, D. J. Lockwood, and J.-M. Baribeau. Phys. Rev. B: Condens. Matter, **41**, 5319 (1990).
16. J. White, G. Fasol, R. Ghanbari, C. J. Gibbings, and C. G. Tuppen. Thin Solid Films **183**, 71 (1989).
17. D. J. Eaglesham and M. Cerullo. Phys. Rev. Lett. **64**, 1943 (1990).

18. J. E. MACDONALD, A. A. WILLIAMS, R. VAN SILFHOUT, J. F. VAN DER VEEN, M. S. FINNEY, A. D. JOHNSON, and C. NORRIS. NATO Advanced Research Workshop on Kinetics of Ordering and Growth at Surfaces. In press.
19. D. KONOGSBERGER and R. PINS (*Editors*). X-ray absorption: principles, techniques and applications of EXAFS and XANES. Academic Press Inc., New York. 1988.
20. P. A. LEE, P. H. CITRIN, P. EISENBERGER, and B. M. KINCAID. Rev. Mod. Phys. **53**, 769 (1981).
21. A. G. MCKALE, B. W. VEAL, A. P. PAULIKAS, S. K. CHAN, and G. S. KNAPP. J. Am. Chem. Soc. **110**, 3763 (1988).
22. A. ERBIL, G. S. CARGILL III, R. FRAHM, and R. F. BOEHME. Phys. Rev. B: Condens. Matter, **37**, 2450 (1988).
23. W. T. ELAM, J. P. KIKLAND, R. A. NEISER, and P. D. WOLF. Phys. Rev. B: Condens. Matter, **38**, 2 (1988).
24. T. TYLISZCZAK, A. P. HITCHCOK, and T. E. JACKMAN. J. Vac. Sci. Technol. A, **8**, 2020 (1990).
25. H. OYANGI, T. SAKAMOTO, K. SAKAMOTO, H. YAMAGUCHI, and T. YAO. Extended Abstracts of the 21st Conference on Solid State Devices and Materials, Tokyo, 1989. Business Center for Academic Societies, Japan. 1989. pp. 509–512.
26. M. ASAI, H. UEBA, and C. TATSUYAMA. J. Appl. Phys. **58**, 2577 (1985).
27. H. J. GOSSMAN, L. C. FELDMAN, and W. M. GIBSON. Surf. Sci. **155**, 413 (1985).
28. S. S. IYER, J. C. TSANG, M. W. COPEL, P. R. PUKITE, and R. M. TROMP. Appl. Phys. Lett. **54**, 219 (1989).
29. K. MIKI, K. SAKAMOTO, and T. SAKAMOTO. Mater Res. Soc. Symp. Proc. **148**, 323 (1989).
30. J.-M. BARIBEAU, R. PASCUAL, and S. SAIMOTO. Appl. Phys. Lett. **57**, 1502 (1990).
31. R. PASCUAL, S. SAIMOTO and J.-M. BARIBEAU. Can. J. Phys. **69**, 241 (1991).
32. A. OURMAZD and J. C. BEAN. Phys. Rev. Lett. **55**, 765 (1985).
33. D. J. LOCKWOOD, K. RAJAN, E. W. FENTON, J.-M. BARIBEAU, and M. W. DENHOFF. Solid State Commun. **61**, 465 (1987).
34. D. E. JESSON, S. J. PENNYCOOK, M. F. CHISHOLM, and J.-M. BARIBEAU. Mater Res. Soc. Symp. **183**, 223 (1990).
35. M. COPEL, M. C. REUTER, E. KAXIRAS, and R. M. TROMP. Phys. Rev. Lett. **63**, 632 (1989).

Can. J. Phys. Downloaded from www.nrcresearchpress.com by Dalian Nationalities University on 06/05/13
For personal use only.

View publication stats